European Journal of Medicinal Chemistry 154 (2018) 220–232

Contents lists available at ScienceDirect

European Journal of Medicinal Chemistry

journal homepage: http://www.elsevier.com/locate/ejmech

Research paper

Two new Cu(II) dipeptide complexes based on 5-methyl-2-(2′-pyridyl) benzimidazole as potential antimicrobial and anticancer drugs: Special exploration of their possible anticancer mechanism

Yong-Yu Qi [a], Qian Gan [a], Ya-Xian Liu [a], Ya-Hong Xiong [a], Zong-Wan Mao [a, b], Xue-Yi Le [a, *]

[a] Department of Applied Chemistry, South China Agricultural University, Guangzhou 510642, PR China
[b] School of Chemistry and Chemical Engineering, Sun yat-sen University, Guangzhou 510275, PR China

ARTICLE INFO

Article history:
Received 12 March 2018
Received in revised form
14 May 2018
Accepted 14 May 2018
Available online 21 May 2018

Keywords:
Cu(II) complexes
DNA interaction
Antimicrobial activity
Cytotoxicity
Anticancer mechanism

ABSTRACT

In the search for more effective anticancer drugs with less toxic side effects, dipeptides were introduced into the Cu(II) complex of 5-methyl-2-(2′-pyridyl)benzimidazole (HPBM). Analytical and spectroscopic techniques were employed to thoroughly characterize complexes [Cu(Gly-gly)(HPBM)(H_2O)]$ClO_4 \cdot 0.5H_2O$ (**1**) and [Cu(Gly-*L*-leu)(HPBM)(H_2O)]ClO_4 (**2**) (where Gly-gly = Glycyl-glycine anion, Gly-*L*-leu = Glycyl-*L*-leucine anion). The solution stability studies performed by ultraviolet–visible (UV–Vis) spectroscopy confirmed the stability of the complexes in the buffer solutions. The DNA binding affinity was evaluated using multi-spectroscopy, viscosity measurement and molecular docking methods and further quantified by K_b and K_{app} values, revealing an intercalative mode. Moreover, gel electrophoresis analysis revealed that the complexes could damage CT DNA through a hydroxyl radical pathway in the presence of ascorbic acid. All the complexes displayed favorable antimicrobial and cytotoxic activities toward the tested microorganisms (*Bacillus subtilis*, *Staphylococcus aureus*, *Escherichia coli* and *Pseudomonas aeruginosa*) and cancer cells (A549, HeLa and PC-3). Most importantly, the possible anticancer mechanism of the complexes was explored by determining the cells morphological changes, intracellular reactive oxygen species (ROS) levels, location in mitochondria, mitochondrial membrane potentials and the expression of Bcl-2 family proteins. The results showed that the complexes could induce apoptosis in HeLa cells through an ROS-mediated mitochondrial dysfunction pathway, which was accompanied by the regulation of Bcl-2 family proteins.

1. Introduction

Based on the wide range of coordination numbers, inconstant geometries and available redox states, metal complexes have become one hotspot in the research of anticancer agents [1–4]. Among various anticancer agents, cisplatin as a potent agent against numerous malignancies has been widely used. But the side effects and drug resistance of cisplatin still limited its clinical applications and future development. Therefore, some strategies based on different metals and ligands were proposed by chemists to search more efficacious anticancer agents with less side effects, in which copper complexes have been clearly considered as the most promising anticancer agents [5–7].

As an endogenous metal element, copper has less toxic side effects compared with exogenous metals (platinum, ruthenium and rhenium etc.) [7]. The unique spectroscopic properties as well as excellent redox properties make its complexes have favorable DNA oxidative cleavage [8] and various biological activities, such as antimicrobial, anticancer and anti inflammatory activities [9–11]. It was reported that the anticancer activity of some copper complexes was more prominent and more effective than that of cisplatin drug, especially for human cancer cell which generates traditional platinum resistance [12]. In this case, copper complexes based on benzimidazole and their derivatives have gained great attention due to their better antimicrobial and anticancer activities [13–17], but some of them still have severe toxic side effects [18].

Dipeptides, formed by the dehydration condensation of two amino acids, are structurally similar to proteins, hence the introduction of dipeptides as an auxiliary ligand could effectively

* Corresponding author.
E-mail address: lexyfu@163.com (X.-Y. Le).

https://doi.org/10.1016/j.ejmech.2018.05.023
0223-5234/

enhance the biological compatibility and recognition of the complexes, and reduce the toxic side effects [19–22]. For instance, the copper-dipeptide complexes, [Cu(Ala-Phe)] (Ala-Phe = L-Alanyl-L-Phenylalanine anion) and [Cu(Phe-Ala)] (Phe-Ala = L-Phenylalanyl-L-Alanine anion), were found to possess effective cytotoxicity against breast cancer and less toxic effects against normal cells [23]. The similar results have been reported in numerous other studies [8,24,25]. Most importantly, it has been found that the activities of ternary copper-dipeptide complexes based on benzimidazole ($[Cu(glygly)(HPB)Cl]\cdot 2H_2O$, HPB = 2-(2′-pyridyl)benzimidazole) [26] were stronger than that of the corresponding binary complex ($[CuCl_2(pbzH)]$, pbzH = 2-(2′-pyridyl)benzimidazole) [27]. Therefore, further study of ternary Cu(II)-dipeptide complexes with benzimidazole derivatives should be favorable for the development of new anticancer drugs with high efficiency and low toxicity.

In our previous work, a series of ternary mixed copper dipeptide complexes based on benzimidazole derivatives, their cytotoxic activities have been reported [28–31]. However, the mechanism of their anticancer action has not been explored. Herein, as our continuous and deep work in this area, two new copper complexes $[Cu(Gly\text{-}gly)(HPBM)(H_2O)]ClO_4\cdot 0.5H_2O$ (**1**) and $[Cu(Gly\text{-}L\text{-}leu)(HPBM)(H_2O)]ClO_4$ (**2**) were synthesized and characterized. The interaction of the complexes with CT DNA was investigated via spectroscopic experiments, hydrodynamics, gel electrophoresis and molecular docking technique. The in vitro cytotoxicity and antimicrobial activity of the complexes were tested by MTT, oxford cup and broth dilution methods, respectively. Most importantly, the possible anticancer mechanism of the complexes was explored by determining the cells morphological changes, intracellular reactive oxygen species (ROS) levels, location in mitochondria, mitochondrial membrane potentials and the expression of Bcl-2 family proteins.

2. Results and discussion

2.1. Synthesis and characterization of the complexes

The syntheses of HPBM and the complexes were schematically presented in Scheme 1. The complexes were characterized by elemental analysis, molar conductivity measurement, and various spectroscopic techniques (IR, UV–Vis, ESI-MS and ESR). The elemental analytic results for the complexes match well with their theoretical values, which confirm the compositions of the complexes. The molar conductivities of complexes **1** and **2** in MeOH are 89.3 and 97.8 $S\,cm^2\,mol^{-1}$, respectively, indicating their 1:1 electrolyte nature [32]. The ESI-MS spectra in MeOH solvent exhibited molecular ion peaks at *m/z* 403.9 and 459.0, matching accurately with $[Cu(Gly\text{-}gly)(HPBM)]^+$ and $[Cu(Gly\text{-}L\text{-}leu)(HPBM)]^+$, respectively.

The IR spectra of complexes **1** and **2** exhibit a broad band at about 3412 cm^{-1} and 3437 cm^{-1}, respectively, which can be ascribed to the stretching vibration $\nu(-OH)$ of the water molecules. Two bands at 3091 and 2925 cm^{-1} for **1** (3082 and 2960 cm^{-1} for **2**) can be assigned to the $\nu_{as}(-NH_2)$ and $\nu_s(-NH_2)$ stretching vibrations, respectively. The peaks around 1610 and 1395 cm^{-1} for **1** (1615 and 1381 cm^{-1} for **2**) are attributed to $\nu_{as}(-COO^-)$ and $\nu_s(-COO^-)$ stretching vibrations of the carboxylate group of the coordinated dipeptide ligand. In addition, the peaks at 1488 cm^{-1} for **1** and 1436 cm^{-1} for **2** can be ascribed to the amide II bands arising out of ν(C–N) and δ(N–H) modes (coupled to one another) [33], indicating that the nitrogen atom of the amide bonds was not deprotonated. Meanwhile, the $\Delta\nu$ values in the range 210–240 cm^{-1} showed a monodentate coordination mode of the carboxylate group of the dipeptides [24]. Further, the peaks at 1456 cm^{-1} for **1** and 1450 cm^{-1} for **2** can be assigned to the ν(C=N) vibrations of HPBM, indicating that HPBM was coordinated to the central Cu(II) ion. Absorption peaks at about 420 and 626 cm^{-1} for **1** (436 and 623 cm^{-1} for **2**) are assigned to the ν(Cu–N) and ν(Cu–O) vibrations.

The electronic spectra of the complexes in MeOH solvent were measured, in which the intense absorption bands at 317 nm ($\varepsilon = 24\,445\ M^{-1}\,cm^{-1}$) for **1** and 323 nm ($\varepsilon = 25\,346\ M^{-1}\,cm^{-1}$) for **2** correspond to $\pi \rightarrow \pi^*$ transitions of HPBM ligand. Moreover, the broad and weak absorption bands in the visible range at 665 nm ($\varepsilon = 74.81\ M^{-1}\,cm^{-1}$) for **1** and 677 nm ($\varepsilon = 64.45\ M^{-1}\,cm^{-1}$) for **2** are assigned to the d→d transition of the Cu(II) ion, suggesting a typically distorted square-pyramidal geometry [19].

The X-band ESR spectra of the complexes in MeOH (100 K) were recorded at 9.46 GHz under the magnetic field strength of 3000 ± 1000 G using tetracyanoethylene (TCNE) as field marker. The ESR spectra display an anisotropy signal with $g_{||} = 2.2784$, $g_{\perp} = 2.0444$, and $A_{||} = 166.030$ for **1** and $g_{||} = 2.2570$, $g_{\perp} = 2.0477$, and $A_{||} = 154.570$ for **2**. The trend $g_{||} > g_{\perp} > g_e$ (2.0023) indicated that the unpaired electron of the Cu(II) ion was located in the d_{x2-y2} orbital, revealing the nearly square-pyramidal geometry of the complexes [34,35].

Based on the above results and relevant literature [26,36,37], an approximate square-pyramidal geometry can be conjectured for the Cu(II) complexes, where the four equatorial positions were occupied by HPBM (N, N) and Gly-gly/Gly-*L*-leu (N, O) and the axial position was occupied by a water molecule. In addition, because HPBM and Bipy are similar bidentate ligands(N, N), we can speculate that the complexes exhibit high stability in aqueous solution, and their species distribution is analogous to complexes [Cu(bipy)(glygly/gly-*L*-leu)] [38], viz., $[Cu(HPBM)(Gly\text{-}Gly/Gly\text{-}L\text{-}Leu)]^+$ and [Cu(HPBM) (Gly-Gly-H/Gly-*L*-Leu-H)] are the main species in solution of the complexes.

The stability of the Cu(II) complexes in Tris-HCl (pH = 7.2) and PBS (pH = 7.8) buffer solutions was studied by UV–Vis spectroscopy at different time intervals. As shown in Fig. S1, no obvious changes were observed in absorbance of the complexes (10 μM) in the Tris-HCl buffer at 0 and 8 min. Likewise, the UV spectra of the complexes (8.2 μM) in the PBS at 0 and 24 h also exhibited no changes. The results suggested that the Cu(II) complexes were stable in both Tris-HCl and PBS buffer solutions.

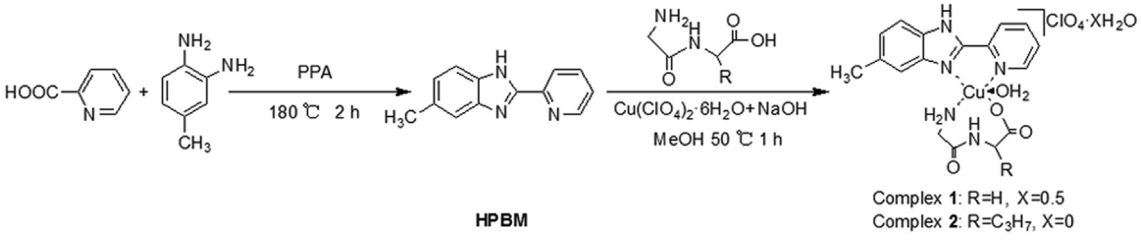

Scheme 1. Synthesis of HPBM, complex **1** and complex **2**.

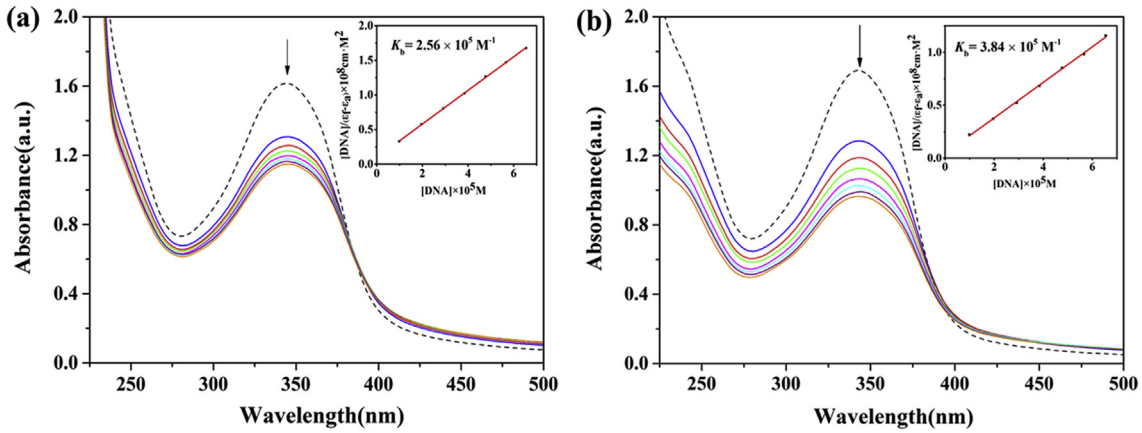

Fig. 1. Electronic absorption spectra of complexes **1** (a) and **2** (b) in 5 mM Tris-HCl buffer upon addition of CT DNA. The arrow indicates the change upon increasing amounts of CT DNA. Inset: Plot of [DNA]/(ε_f-ε_a) vs. [DNA] for the titration of CT DNA with complex, and the binding constants (K_b) were calculated using Eq. (1).

2.2. Complexes-CT DNA binding studies

The absorption spectra of the complexes were recorded in the absence and presence of CT DNA at different *r* values ([complex]/[DNA]). As depicted in Fig. 1, with the addition of CT DNA, the spectra of the complexes exhibit a slight red shift and hypochromic effect (hypochromism, 27.03% for **1** and 43.15% for **2**). The spectral changes clearly show that the complexes could interact with DNA through an intercalative mode [39]. In order to quantify the DNA binding affinities of the complexes, the binding constants (K_b) were determined using Eq. (1) (Experimental part). The obtained K_b values of the complexes were $2.56 \times 10^5\ M^{-1}$ for **1** and $3.84 \times 10^5\ M^{-1}$ for **2**, respectively, which were less than that of the classical intercalator EB ($1.4 \times 10^6\ M^{-1}$) [26], but was higher than that of complex [Cu(Gly-Val)(phen)] (Gly-Val = L-Glycyl-L-Valine anion) ($6.2 \times 10^4\ M^{-1}$) [25]. In addition, the binding ability of **2** is stronger than that of **1**, which may be mainly attributed to the side chain length of dipeptides. The longer the side chain is, the stronger the hydrophobicity of the complex, thereby resulting in a higher binding affinity.

Competitive binding experiments were carried out to further verify the interaction between the complexes and CT DNA. The fluorescence emission spectra of EB-CT DNA (EB = 8 μM, [DNA] = 10 μM) in the absence and presence of the complexes were recorded. As shown in Fig. 2, on addition of the complexes at different *r* values, the fluorescence intensity of the EB-CT DNA system at 525 nm was decreased, indicating that the complexes could replace EB to bind to CT DNA, which further confirmed that the complexes interact with CT DNA via the intercalative mode (Fig. 2) [40]. The Stern–Volmer quenching constants (K_{SV}) were calculated using Eq. (2) (Experimental part). The obtained K_{sv} values for the complexes at 300 K were $1.64 \times 10^4\ M^{-1}$ for **1** and $1.90 \times 10^4\ M^{-1}$ for **2**, respectively, The DNA-binding affinities follow the order **2** > **1**. Additionally, the K_{app} values for complexes **1** and **2** were calculated to be $1.16 \times 10^6\ M^{-1}$ and $1.32 \times 10^6\ M^{-1}$ using Eq. (3) (Experimental part), indicating that the DNA binding ability of **2** was stronger than that of **1**.

CD spectroscopy is an effective method for monitoring CT DNA conformational changes during small molecule-DNA interactions. The observed CD spectrum of CT DNA consists of two bands, a positive band at 274 nm due to base-pair stacking and a negative one at 246 nm due to right-hand helicity of B-DNA, and these bands are quite sensitive to the interaction mode between small molecules and DNA [41,42]. The results showed that, on the addition of the complexes to CT DNA solution, the CD absorption band strengths of the DNA were decreased with an obvious red shift (Fig. S2). The change of the positive band strength was significantly higher than that of the negative band (that is, the change of the base-pairs stacking strength was greater than that of the right-hand helix), suggesting the complexes may mainly inserted into the base-pairs of CT DNA, which unwound the double helix of the DNA, thus, weakened the strength of the bands. Moreover, the

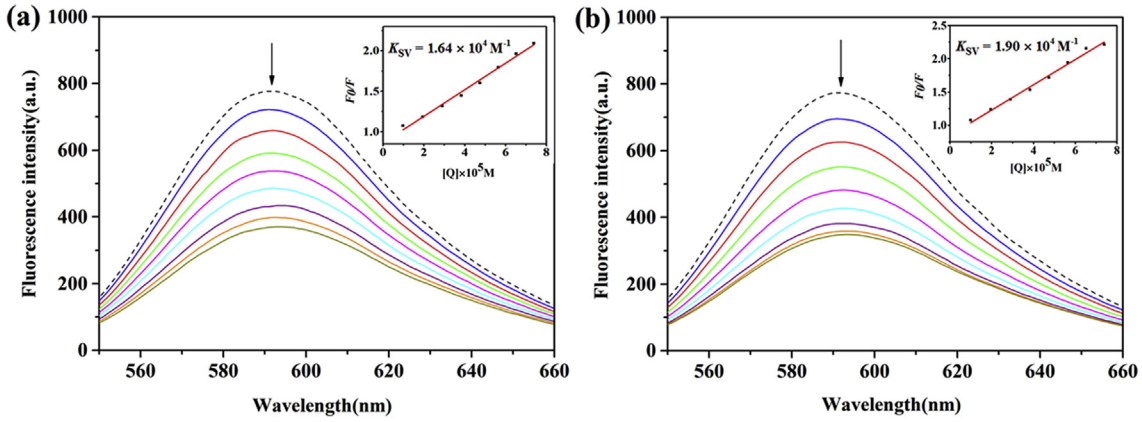

Fig. 2. Fluorescence emission spectra of the CT DNA-EB system with increasing amounts of complexes **1** (a) and **2** (b). The arrow shows the intensity change upon increasing concentration of the complexes. Inset: Plot of F_0/F vs. [Q] for the titration of the complexes, and the Stern–Volmer constants (K_{SV}) were calculated using Eq. (2).

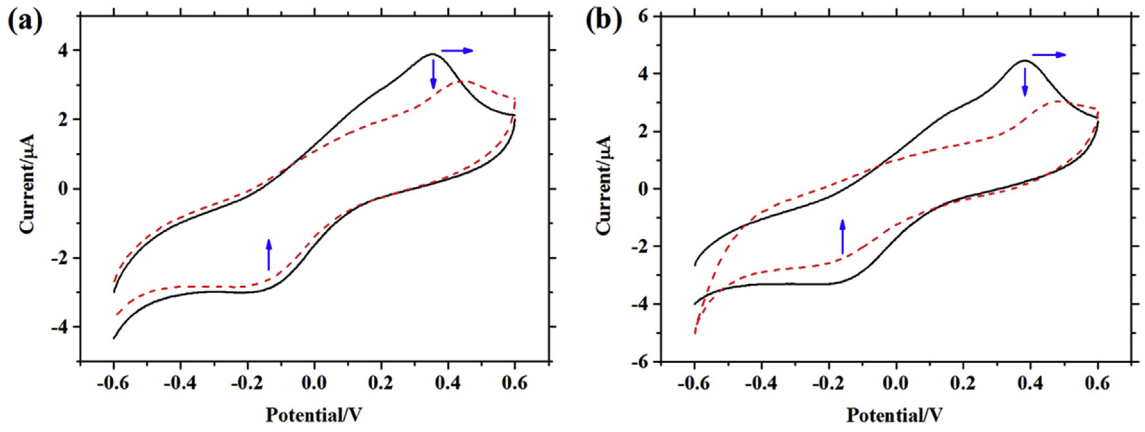

Fig. 3. Cyclic voltammograms of complexes **1** (a) and **2** (b) in the absence and presence of CT DNA (0.9 mM) at 200 mV s^{-1} scan rate.

intensity changes follow the trend **2** > **1**, indicating that the DNA binding ability of **2** is stronger than that of **1**.

Electrochemical measurement can be used in the investigation of the interaction between the complexes and CT DNA, which can provide a valuable supplement to the above mentioned spectroscopic titration experiments, and further confirm the binding mode of the complexes to CT DNA. In general, the electrochemical potential of a complex will shift positively when it intercalates into the double helix of CT DNA, while the potential will shift to the negative direction in the case of electrostatic interaction [43]. The cyclic voltammograms of the Cu(II) complexes (Fig. 3) were recorded in the absence and presence of CT DNA and the relevant data were presented in Table 1. The ratios of the oxidation peak and reduction peak (*I*pa/*I*pc) are close to 1, indicating that the redox process is quasi-reversible [44]. Upon addition of CT DNA to the complexes, the current intensity of all the peaks weakened obviously and no new redox peaks appeared, showing that the complexes bound strongly to the DNA. The reduction in current can be attributed to the decrease of the concentration of electrochemically active substance, which may be due to the non-electrochemical activity of the combination product of the complexes with the DNA. In the presence of CT DNA, the anodic potential and condition potential were shifted positively, indicating that the binding mode of the complexes with the DNA was an intercalative mode.

In addition, the ratios of binding constants of the reduced state Cu(I) and oxidized state Cu(II) complexes were calculated using Eq. (3) (Experimental part). The obtained $K_{Cu(I)}/K_{Cu(II)}$ values of the complexes were 4.95 for **1** and 8.90 for **2**, respectively, indicating that the DNA binding ability of the Cu(I) states for the complexes was stronger than that of their corresponding Cu(II) states. Furthermore, with the addition of CT DNA, the peak currents were decreased significantly and the peak potential was shifted positively, in which the shift of **2** was greater than that of **1**, suggesting the binding affinities of the complexes with DNA follow the order **2** > **1**. The result was consistent with that of the above spectral experiments.

Table 1
The cyclic voltammetry data for the complexes in the absence and presence of CT DNA.

Compounds	E_{pa} (V)	E_{pc} (V)	ΔE (V)	$E_{1/2}$ (V)	I_{pa}/I_{pc} (V)	$K_{Cu(I)}/K_{Cu(II)}$ (V)
1	0.355	−0.177	0.532	0.089	1.301	4.95
1 + CT DNA	0.435	−0.176	0.611	0.130	1.120	
2	0.381	−0.204	0.585	0.089	1.347	8.90
2 + CT DNA	0.483	−0.194	0.677	0.145	1.187	

DNA viscosity is quite sensitive to DNA length changes, thus, its measurements are usually regarded as the most critical method to detect the binding mode of small molecules with DNA in the absence of crystallographic structural data [43]. In the case of the classic intercalation, the DNA helix increases as base pairs are separated to accommodate the bound compound resulting in increase of the DNA viscosity. However, a partial or non-classic intercalation will lead the DNA helix to bend or kink reducing its valid length and, as a result, the relative viscosity of DNA is decreased slightly or remains unchanged [45]. Viscosity measurements were carried out on CT DNA solutions (200 μM) upon addition of the complexes (Fig. S3). The relative viscosity of CT DNA showed a steady increase with the addition of the complexes, indicating that the binding mode between the DNA and complexes was an intercalative mode. The increased degree of the viscosity was closely related to the DNA affinity, following the order **2** > **1**,

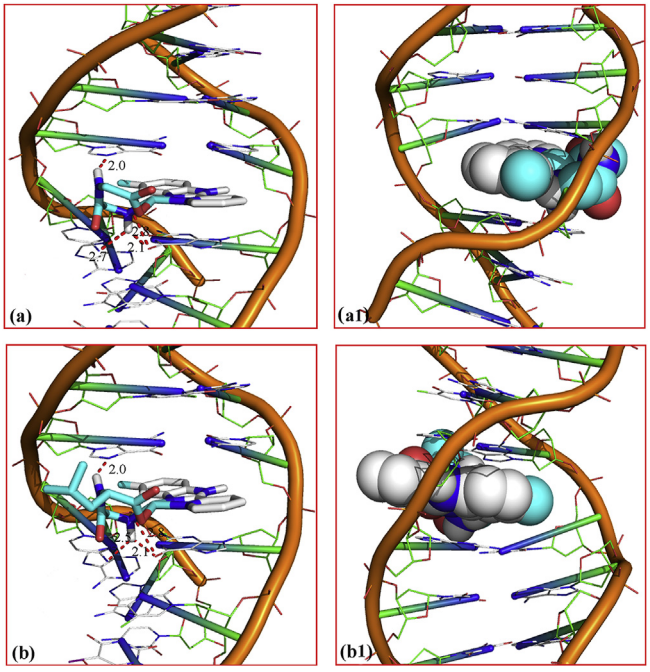

Fig. 4. Molecular docked models of complexes **1** (a) and **2** (b) with DNA. The hydrogen bonds of the complexes (showing stick representation) and DNA (cartoon form) are expressed as red dashed lines. (For interpretation of the references to color in this figure legend, the reader is referred to the Web version of this article.)

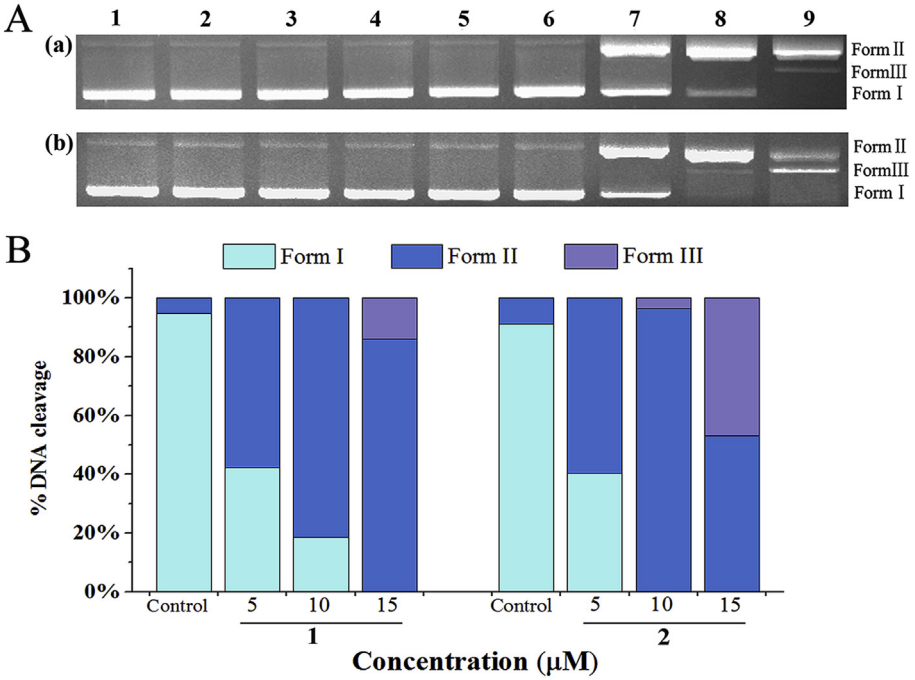

Fig. 5. (A) The cleavage of pBR322 DNA (250 ng) by complexes **1** (a) and **2** (b) with 1 h incubation in the presence of ascorbic acid (50 μM). Lane 1, DNA control; lane 2, DNA + ascorbic acid (50 μM); lane 3, DNA + $Cu(ClO_4)\cdot 6H_2O$ (20 μM); lane 4, DNA + HPBM (20 μM); lane 5, DNA + Gly-gly/Gly-*L*-leu (20 μM); lane 6, DNA + **1**/**2** (20 μM); lanes 7–10, DNA + ascorbic acid (50 μM) + **1**/**2** (5, 10, 15 and 20 μM, respectively). (B) The DNA cleavage percentages of the complexes (5–15 μM) after incubation for 1 h at 37 °C.

which was uniform with the results obtained from the above studies.

To further understand the interactions between the complexes and DNA, molecular docking simulations were performed with the double strand DNA of the sequence d(5′-G-dIU-TGCAAC-3′) (PDB ID: 454D). It is obvious from Fig. 4 that the complexes were inserted into the empty cavity within GC/GC base pairs rich region from the DNA central position via the non-water soluble aromatic heterocyclic ligand. Thus, the hydrophobic interaction was the major force. Furthermore, the same amounts of hydrogen bonds were formed between the complexes and DNA bases, including complex **1**: H14…454D: DG-4:N7 (2.0 Å), complex **1**: H13…454D: DG-12:O6 (2.8 Å), complex **1**: H19…454D: DC-5:N4 (2.7 Å) and complex **1**: H19 …454D: DG-12:O6 (2.1 Å) as well as complex **2**: H18…454D: DG-4:N7 (2.0 Å), complex **2**: H19…454D: DG-12:O6 (2.8 Å), complex **2**: H24…454D: DC-5:N4 (2.5 Å) and complex **2**: H24…454D: DG-12:O6 (2.1 Å). The relative binding energies of the docked complexes were found to be −35.56 (**1**) and −37.66 kJ mol^{-1} (**2**), respectively. The more negative the relative binding energy, the higher the binding affinity. Therefore, **2** has better DNA binding affinity compared with **1**, which is consistent with the above experimental results.

2.3. Gel electrophoresis analysis

The DNA cleavage of the complexes against plasmid pBR322 DNA was monitored using agarose gel electrophoresis method in the absence and presence of ascorbic acid (50 μM). It is evident that the complexes could cleave CT DNA efficiently in a concentration-dependent manner in the presence of ascorbic acid (Fig. 5A and B), but in the control experiments, ascorbic acid/the ligands/the corresponding complexes alone exhibited no remarkable cleavage activity. The cleavage efficiency was defined by testing the ability of the complexes to transform the supercoiled DNA to nicked circular form (Form II) or linear form (Form III). Evidently, under the same experimental conditions, complex **2** showed a higher cleavage ability compared with complex **1**, which may be linked to the higher DNA binding affinity and Cu(II)/Cu(I) redox potential of the former.

The oxidative cleavage DNA of the complexes may involve multiple reactive oxygen species such as hydroxyl radical (·OH), singlet oxygen ($^1O_2$) and superoxide anion ($\cdot O_2^-$). To elucidate the potential mechanism of the DNA cleavage activity, some standard radical scavengers were introduced into DNA solution, respectively, before the complexes and ascorbic acid were added (Fig. 6A and B). The results showed that, when DMSO, *tert*-butyl alcohol and EtOH (hydroxyl radical scavengers) was added respectively, the cleavage activity was obviously inhibited (lane 4–6), revealing that the cleavage process involved ·OH radicals. On the other hand, the addition of NaN_3 (singlet oxygen quencher) to the reaction mixture exhibited no significant inhibition of the cleavage (lane 7), suggesting that $^1O_2$ was not involved in the process. Furthermore, the adding of SOD (superoxide anion scavenger) could promote the cleavage process (lane 8), indicating that $\cdot O_2^-$ was indirectly involved in the cleavage process, in which the Cu(II) complexes could catalyze the dismutation of $\cdot O_2^-$ to generate H_2O_2 and Cu(I) complexes leading to further damage to the DNA, which is similar to the mechanism of Cu(II)·Val-Pro complex (Val-Pro = Valyl-L-Proline anion) proposed by Arjmand [24].

2.4. Antimicrobial activity

The antimicrobial activities of the complexes and corresponding ligands were evaluated against two Gram(+) (*B. subtilis* and *S. aureus*) and two Gram(−) (*E. coli* and *P. aeruginosa*) microorganisms by monitoring the bacteriostatic circles and MIC values [46].

The diameters of inhibition zones (mm) obtained are listed in Table 2. The results showed that the complexes were active against all the tested bacteria and the activities were much higher than those of the corresponding ligands, which may be

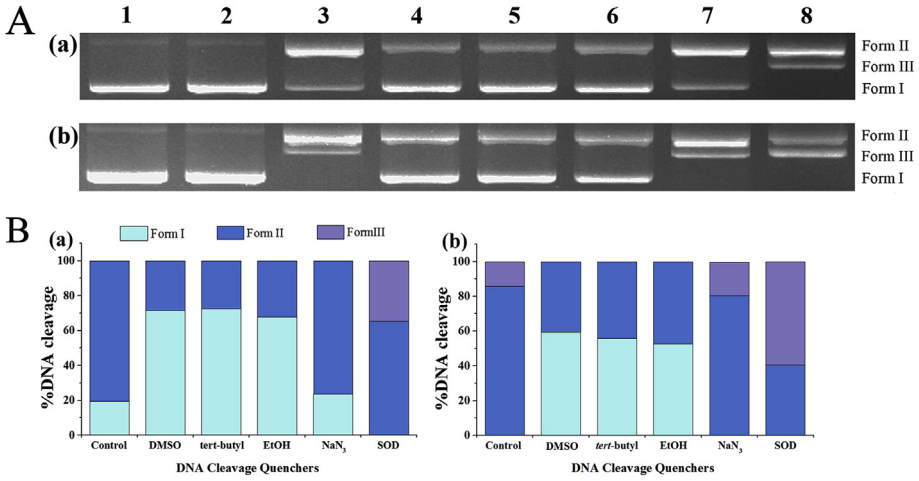

Fig. 6. **(A)** The cleavage of pBR322 DNA (250 ng) by complexes **1** (a) and **2** (b) with 1 h incubation in the presence of different typical reactive oxygen species scavengers. Lane 1, DNA control; Lane 2, DNA + ascorbic acid (50 μM) + SOD (15 units); Lane 3, DNA + ascorbic acid (50 μM) + **1**/**2** (10 μM); Lanes 4–8, DNA + ascorbic acid (50 μM) + **1**/**2** (10 μM) + [DMSO (0.2 M), *tert*-butyl alcohol (0.2 M), EtOH (0.2 M), NaN_3 (0.2 M) and SOD (15 units), respectively]. (B) The DNA cleavage percentages of the complexes (10 μM) after incubation for 1 h at 37 °C in the presence of different typical reactive oxygen species scavengers. The scavengers concentrations were: DMSO (0.2 M), *tert*-butyl alcohol (0.2 M), EtOH (0.2 M), NaN_3 (0.2 M) and SOD (15 units).

Table 2
Antimicrobial activities of the complexes and their ligands against *B. subtilis*, *S. aureus*, *E.coli* and *P. aeruginosa* evaluated by the inhibition zone diameter (mm).

Compounds	Diameter of inhibition zone (mm)			
	B. subtilis	*S. aureus*	*E. coli*	*P. aeruginosa*
Complex **1**	28.1 ± 0.8	23.0 ± 1.0	22.0 ± 0.6	14.0 ± 0.3
Complex **2**	37.0 ± 0.5	30.0 ± 0.7	28.0 ± 0.8	19.0 ± 0.4
HPBM	12.0 ± 0.3	11.0 ± 0.2	9.0 ± 0.5	9.0 ± 0.2
Gly-gly	8.0 ± 0.4	6.0 ± 0.3	7.0 ± 0.2	8.0 ± 0.2
Gly-*L*-leu	9.0 ± 0.2	7.0 ± 0.3	8.0 ± 0.2	9.0 ± 0.3
$Cu(ClO_4)_2{\cdot}6H_2O$	21.0 ± 0.2	19.0 ± 0.3	15.0 ± 0.5	11.0 ± 0.4

due to the synergetic effect caused by their coordination. The sensitivity rank of microorganisms of the complexes was *B. subtilis* > *S. aureus* > *E. coli* > *P. aeruginosa*, revealing the complexes were more sensitive toward Gram-positive bacteria. In addition, the antimicrobial ability of **2** was appreciably higher than that of **1**, which was consistent with the higher DNA binding and efficient oxidative DNA cleavage abilities. Therefore, we can presume that the complexes may hinder the DNA replication by binding and oxidatively damaging DNA, and then inhibit the growth of bacteria [47].

In addition, it can be found from Table 3 that the inhibition of complex 2 against *S. aureus* was higher than that of Gentamycin and Ampicillin used widely [48,49], indicating that the complex has the potential as drug of antibacterial activity against Gram-positive bacteria.

2.5. Cytotoxicity in vitro

The MTT assay was used to evaluate the cytotoxic activities of the complexes against A549, HeLa, PC-3 cancer cells and human normal hepatocyte LO_2 cells, with cisplatin as a positive control. The IC_{50} values are listed in Table 4. Evidently, complex **2** exhibited stronger cytotoxicity than **1** toward all the tested cancer cells, which may be due to the higher DNA binding/cleavage ability of **2**. Importantly, the cytotoxicity of complexes **1** and **2** was higher than that of cisplatin, $[Cu(Gly\text{-}L\text{-}leu)(pbt)(H_2O)]\cdot ClO_4$ ($IC_{50} = 42.6 \pm 2.7$ μM) [29], $[Cu(PBO)(Gly\text{-}L\text{-}leu)(H_2O)]\cdot ClO_4$ ($IC_{50} = 70.8 \pm 2.8$ μM) [30], $[Cu(PBO)(Gly\text{-}gly)(H_2O)]\cdot ClO_4\cdot 1.5H_2O$ ($IC_{50} = 98.6 \pm 6.9$ μM) [30] and $[Cu(glygly)(pbt)(H_2O)]\cdot ClO_4$ ($IC_{50} = 73.6 \pm 3.0$ μM) [28] toward HeLa cells under the same conditions, and the two complexes showed lower cytotoxic effect against the normal LO_2 cells, indicating that the complexes exhibit the potential as effective anticancer drugs against HeLa cells. Since HeLa cells were more sensitive to the complexes, the cancer cell line was selected to perform the following experiments to explore the anticancer mechanism of the complexes.

2.6. Possible anticancer mechanism of the complexes

2.6.1. Apoptosis detection using AO/EB and Annexin V/PI methods

Apoptosis induced by the complexes in HeLa cells was examined using both qualitative and quantitative methods. The changes in the nuclear morphology of HeLa cell were investigated

Table 3
Antimicrobial activities (MIC, MBC in μg mL^{-1}) of the complexes and their ligands against *B. subtilis*, *S. aureus*, *E.coli* and *P. aeruginosa*.

Compounds	*B. subtilis*		*S. aureus*		*E. coli*		*P. aeruginosa*	
	MIC	MBC	MIC	MBC	MIC	MBC	MIC	MBC
Complex **1**	20	25	25	40	80	256	50	64
Complex **2**	8	12.5	16	16	32	200	20	25
HPBM	64	512	320	> 512	512	> 512	64	> 512
Gly-gly	> 512	> 512	> 512	> 512	> 512	> 512	> 512	> 512
Gly-*L*-leu	> 512	> 512	> 512	> 512	> 512	> 512	> 512	> 512
$Cu(ClO_4)_2{\cdot}6H_2O$	300	320	320	400	512	> 512	320	512
Gentamycin [48]	ND	ND	25	ND	ND	ND	17	ND
Ampicillin [49]	ND	ND	312.5	ND	19.53	ND	ND	ND

ND = no detection.

Table 4
The IC_{50} values of the compounds toward the tested cell lines.

Compounds	IC_{50} (μM)			
	A549	PC-3	HeLa	LO_2
HPBM	> 100	> 100	> 100	> 100
Complex **1**	8.58 ± 0.5	16.33 ± 0.2	11.67 ± 0.8	38.02 ± 1.4
Complex **2**	8.39 ± 0.4	11.49 ± 0.6	7.88 ± 0.3	34.67 ± 0.5
Cisplatin	22.67 ± 1.7	18.17 ± 1.4	15.42 ± 3.7	ND
[Cu(PBO)(Gly-gly)(H_2O)]·ClO_4·1.5H_2O [30]	68.14 ± 1.8	93.44 ± 5.8	98.63 ± 6.9	ND
[Cu(PBO)(Gly-*L*-Leu)(H_2O)]·ClO_4 [30]	62.61 ± 0.8	86.52 ± 5.0	70.82 ± 2.8	ND
[Cu(Gly-*L*-Leu)(pbt)(H_2O)]·ClO_4 [29]	38.00 ± 3.2	ND	42.60 ± 2.7	ND
[Cu(gly gly)(pbt)(H_2O)]·ClO_4 [28]	101.16 ± 0.9	17.78 ± 1.2	73.62 ± 3.0	ND

ND = no detection.

using AO/EB staining after the cells were treated with the complexes for 24 h. As shown in Fig. 7A, the living cells in the control showed uniform light green fluorescence, while the treated cells exhibited bright green fluorescence, and some apoptotic features such as nuclei condensation and chromatin alteration were observed. The results demonstrate that the complexes can induce apoptosis in HeLa cells.

In order to further quantitatively compare the effect of the two complexes on the apoptosis, flow cytometry technique was employed to determine the percentage in the early apoptotic cells. As shown in Fig. 7B, the percentage in the early apoptosis was increased in the presence of the complexes (3.69% for control group, 5.71% for **1** and 9.10% for **2**, respectively), indicating that the complexes could induce early apoptosis in cells, and the apoptosis effects follow the order **2** > **1**.

2.6.2. Intracellular ROS levels

According to the results of gel electrophoresis analysis, the complexes could oxidatively damage CT DNA through a hydroxyl radical pathway in the presence of ascorbic acid. However, some studies have confirmed that Cu(II) complexes can induce apoptosis in cancer cells by increasing the level of intracellular ROS [50,51]. Here, the ROS levels in HeLa cells in the absence and presence of the complexes were analyzed using 2′,7′-dichlorodihydrofluorescein diacetate (DCFH-DA) as a fluorescent probe. As shown in Fig. 8A, the dichlorofluorescein (DCF) fluorescence level in the treated cells was markedly increased compared with that in the untreated cells. In addition, the quantitative analysis of the ROS level was carried out, as shown in Fig. 8B. It is found that the DCF fluorescent intensity in the treated cells increased by 2.51 times for **1** and 2.65 times for **2** compared to the control group, indicating that the complexes could

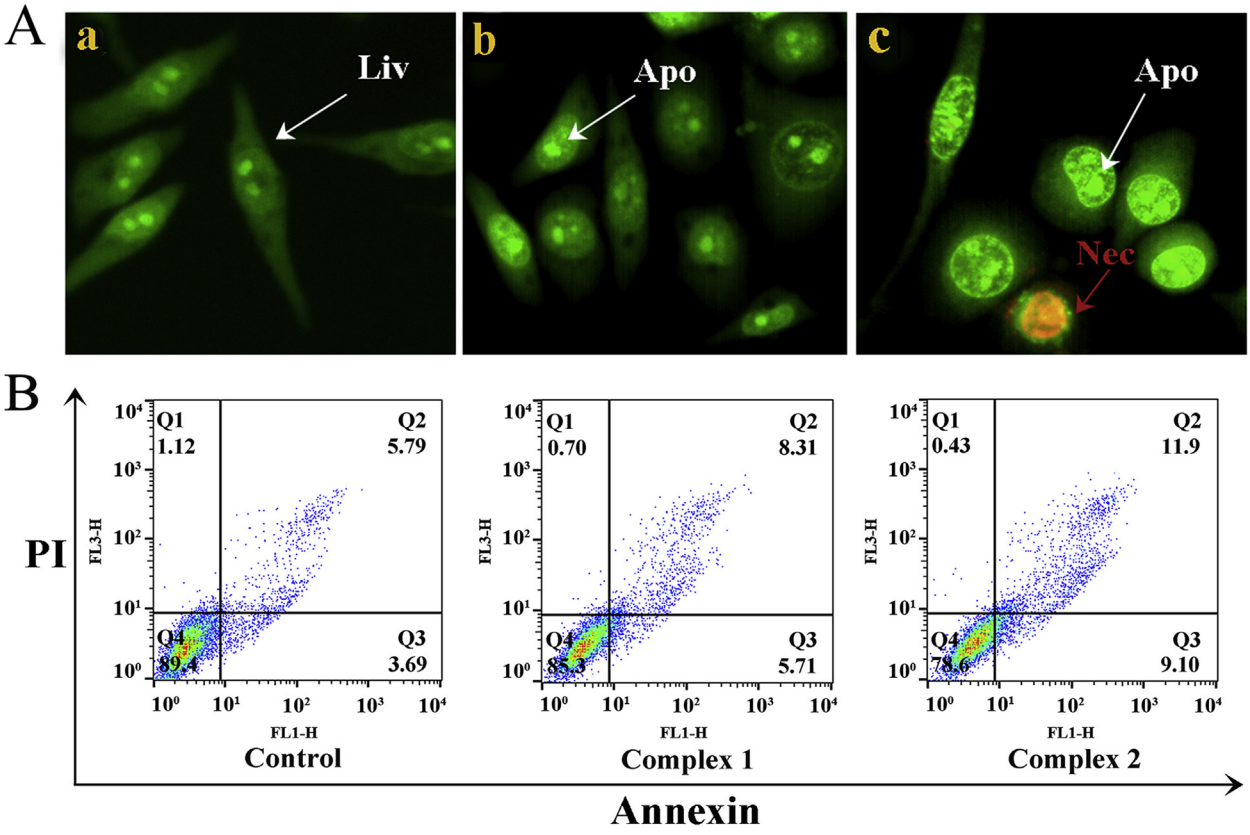

Fig. 7. HeLa cells (a) were treated with the IC_{50} concentrations of complexes **1** (b) and **2** (c) for 24 h at 37 °C. (A) Apoptosis morphological changes were stained with AO/EB. (B) Apoptosis rate was obtained by Annexin V-FITC/PI double staining.

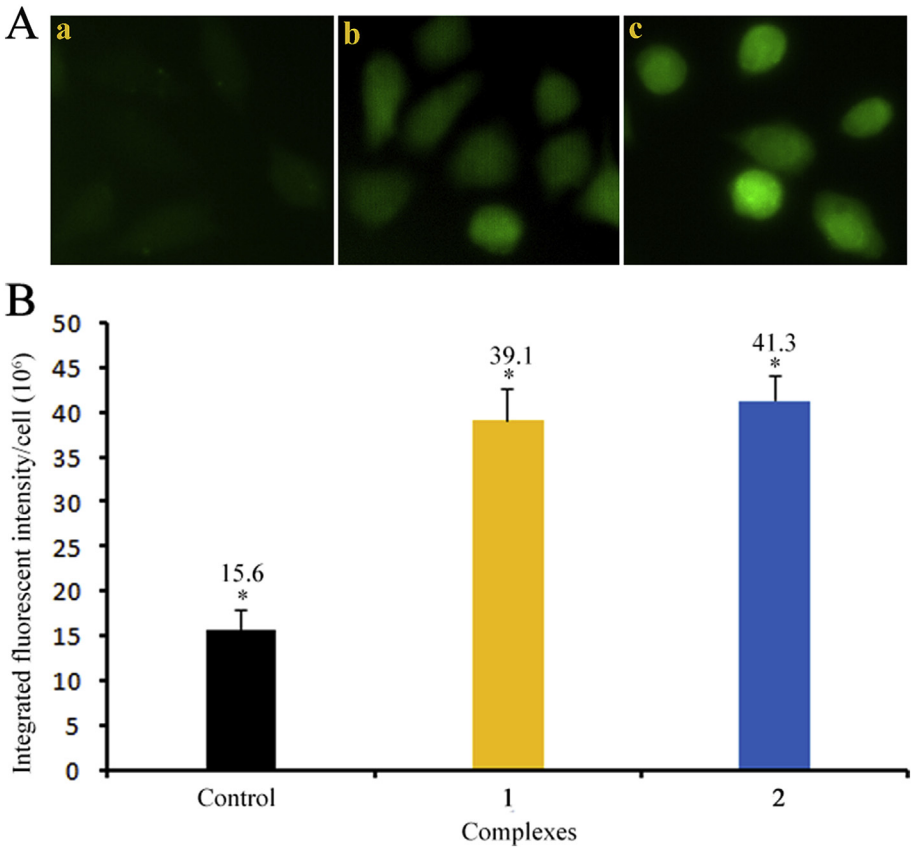

Fig. 8. HeLa cells (a) were treated with the IC_{50} concentrations of complexes **1** (b) and **2** (c) for 24 h at 37 °C. (A) Generation of intracellular ROS induced by the complexes. (B) ROS levels in HeLa cells induced by the complexes were quantitatively analyzed.

observably increase the ROS level in HeLa cells, following the trend **2** > **1**.

2.6.3. Location assay of the complexes and mitochondrial membrane potential (MMP) analysis

As the power house of cells, mitochondria not only provide energy for the cells, but also play an important role in cell apoptosis [52,53]. Additionally, the change of mitochondrial membrane potential also is a key event in the process of apoptosis [4,54]. Thus, in order to understand the mechanism of apoptosis, the location of the complexes in mitochondria and the mitochondrial membrane potential were investigated. The location of the complexes in mitochondria was measured using Mito Tracker® Deep Red FM as a red fluorescent probe. As shown in Fig. 9A, the mitochondria were labeled in red in the control, and the two Cu(II) complexes emitted green fluorescence after the HeLa cells were treated with the complexes for 24 h. The merge of the red and green fluorescence demonstrate that the complexes could enter the cytoplasm through the cell membrane and accumulate in the mitochondria with a time-dependent manner.

Mitochondrial membrane potential (MMP) was assayed using JC-1 as a fluorescent probe. As observed in Fig. 9B, red fluorescence was observed in the control group corresponding to a high mitochondrial membrane potential. However, the complexes-treated cells emitted green fluorescence corresponding to a low mitochondrial membrane potential. The fluorescent change from red to green revealed that the complexes could induce a decrease in the mitochondrial membrane potential. To further quantitatively evaluate the effect of the two complexes on the MMP, the ratios of red/green fluorescent intensity were determined by flow cytometry technique. As shown in Fig. 9C, the red/green ratio in the control group was 11.49%, but when the cells were exposed to the complexes for 24 h, the ratios decreased by 8.56% for **1** and 10.28% for **2**, respectively. These results show that the complexes can induce a decrease in the mitochondrial membrane potential.

2.6.4. Western blot analysis

Apoptosis as one of the processes of the programmed cell death, is associated with the activation, expression and regulation of a series of gene. To investigate the mechanism of the apoptosis induced by the complexes, HeLa cells were treated with 8.2 μM complex for 24 h and the expression of PARP, Caspase-3, Bcl-2, Bad, Bax and p53 was assayed by western blot analysis. As shown in Fig. 10, when the cells were treated with the complexes for 24 h, the expression levels of p53 and pro-apoptotic proteins Bad and Bax were upregulated, whereas the level of anti-apoptotic protein Bcl-2 was downregulated. Besides, the upregulation of caspase-3 and the PARP cleavage were observed. These results indicated that the complexes could induce apoptosis in HeLa cells through the intrinsic pathway, as shown in Fig. 11.

3. Conclusions

Two mixed-ligand copper(II) complexes [Cu(Gly-gly)(HPBM)(H_2O)]ClO_4·0.5H_2O (**1**), [Cu(Gly-*L*-leu)(HPBM)(H_2O)]ClO_4 (**2**) were synthesized and well characterized. The complexes could bind to CT DNA through an intercalation mode, in which hydrophobic interactions were dominant. The binding sites and modes were further confirmed by molecular docking techniques. DNA cleavage experiments revealed that the complexes could

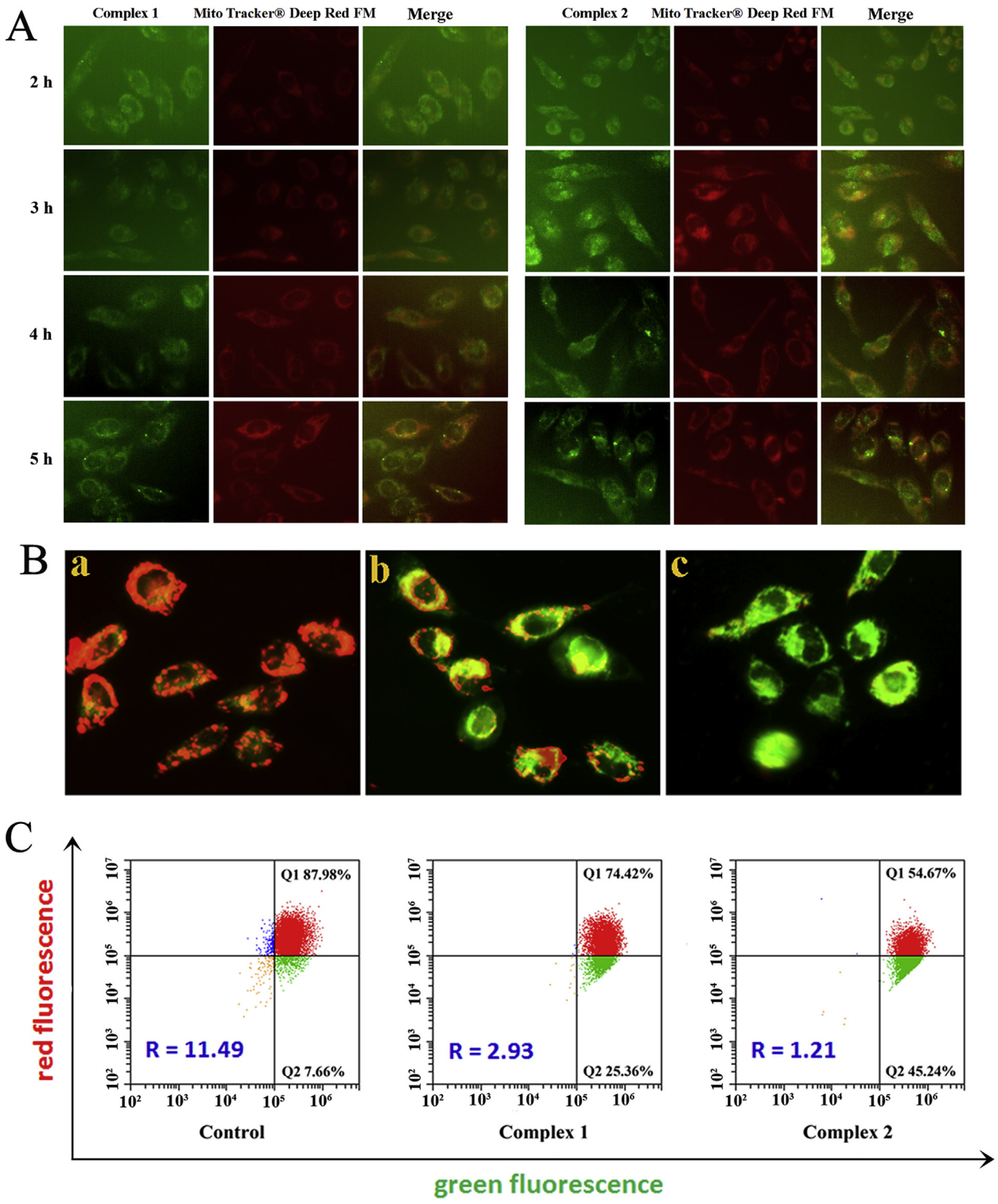

Fig. 9. (A) The mitochondrial location of the complexes. HeLa cells treated with the complexes for 2, 3, 4 and 5 h respectively, and the cells were stained with Mito Tracker® Deep Red FM and then imaged with a fluorescent microscope. (B) Effects of the complexes on mitochondrial membrane potential analyzed by JC-1 staining. HeLa cells (a) were treated with the IC_{50} concentrations of complexes **1** (b) and **2** (c) for 24 h. (C) The ratio of red/green JC-1 fluorescent intensity was monitored by flow cytometry. (For interpretation of the references to color in this figure legend, the reader is referred to the Web version of this article.)

oxidatively damage CT DNA in the presence of ascorbic acid. In addition, all the complexes displayed excellent antimicrobial activity and cytotoxicity toward the tested microorganisms and cancer cells, respectively. The cytotoxicity of complex **2** was stronger than that of complex **1**, which may be mainly attributed to the stronger hydrophobicity of Gly-*L*-leu compared with Gly-gly. Further anticancer mechanistic studies showed that the complexes could induce the apoptosis of HeLa cells, which was further confirmed by the changes in cell morphology and Annexin V positivity. Moreover, it was found that the increase of ROS levels, loss of

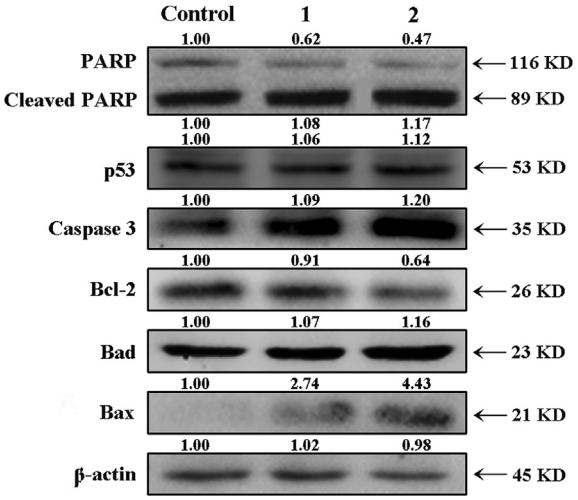

Fig. 10. Western blot analysis of Cleaved PARP, p53, Caspase 3, Bcl-2, Bad and Bax in HeLa cells treated with the IC_{50} concentrations of the complexes for 24 h β-actin was used as the internal reference.

mitochondrial membrane potential, activation of Caspase-3 as well as expression of Bcl-2 family proteins were all related to the apoptosis of the cells. In summary, the complexes induced apoptosis of the cancer cells through the ROS-mediated mitochondrial dysfunction pathway. This work should prove valuable for the rational design and development of new Cu(II) complexes as potent antimicrobial and/or anticancer agents.

4. Experimental

4.1. Materials and methods

All reagents were of commercial reagent grade and were used without further purification, and deionized water was used throughout the experiments. The 5-methyl-2-(2′-pyridyl)benzimidazole was synthesized according to the reported method [55]. The ligands glycyl-glycine and glycyl-L-leucine were purchased from Aladdin. CT DNA, ethidium bromide (EB = 3,8-diamino-5-ethyl-6-phenyl-phenanthridinium bromide), dimethylsulfoxide (DMSO), RPMI-1640 and DMEM were purchased from sigma, and pBR322 DNA was provided by MBI Fermentas (Lithuania). MTT was obtained from Sinopharm Chemical Reagent Co., Ltd. (Shanghai, China). A549 (Human lung carcinoma cell line), HeLa (human cervical carcinoma cell line), PC-3(human prostate carcinoma cell line) and LO_2 (human normal liver cell line) were purchased from the Laboratory Animal Center of Sun Yat-Sen University (Guangzhou, China). *Bacillus subtilis* (*B. subtilis*), *Staphylococcus aureus* (*S. aureus*), *Escherichia coli* (*E. coli*) and *Pseudomonas aeruginosa* (*P. aeruginosa*) were generously provided by the key laboratory of plant molecular breeding of Guangdong province, College of agriculture, South China Agricultural University.

Stock solution of CT DNA was prepared in a buffer solution (pH 7.2) containing 5 mM Tris-HCl and 50 mM NaCl, and stored at 4 °C for no more than 3 days. The DNA concentration in base pairs was determined by UV absorbance at 260 nm ($\varepsilon = 6600\ M^{-1}\ cm^{-1}$). The ratio A_{260}/A_{280} was about 1.8–1.9, indicating that the DNA was sufficiently free of protein [56]. Elemental analysis (C, H, and N) was carried out with a Vario EL elemental analyzer (Elementar, Germany). FI-IR spectra of compounds were recorded on a VERTEX 70 FT-TR spectrometer (Bruker, Germany) in the range of 4000–400 cm^{-1} using KBr pellet method. Molar conductivities were measured on a DDS-11A digital conductance (LeiCi, Shanghai) in 10^{-3} M methanol solution. Electrospray ionization mass (ESI-MS), Electron spin resonance (ESR), UV–vis and fluorescence spectra were recorded on API4000 triple quadrupole mass spectrometer (AB Sciex, USA), Bruker EMX A300 spectrometer (Bruker, Germany), Pharmacia 2550 spectrophotometer (Shimadzu, Japan) and Hitachi F-4500 fluorescence spectrophotometer (Hitachi, Japan), respectively. Circular dichroism spectra were obtained on Chirascan CD spectropolarimeter (Applied Photophysics Ltd., UK). Cyclic voltammetry experiments were carried out using a CHI660A Electrochemical Workstation with glass carbon electrode working electrode, Pt-wire as the auxiliary electrode and saturated calomel electrode (SCE) as the reference electrode.

4.2. Stability of the Cu(II) complexes in solution

All the complexes were dissolved in DMSO (0.5% of the final volume) and then diluted with Tris-HCl and PBS buffer solutions, respectively, to a required concentration. Since 8 min and 24 h of incubations were carried out respectively in the processes of DNA binding and biological activity studies, the time intervals were selected as 8 min for the Tris-HCl buffer solution and 24 h for the PBS buffer solution. The stability of the Cu(II) complexes in solution was investigated by monitoring their UV spectra.

4.3. Synthesis of the complexes

Gly-gly/Gly-*L*-leu (0.066 g/0.094 g, 0.5 mmol) and NaOH

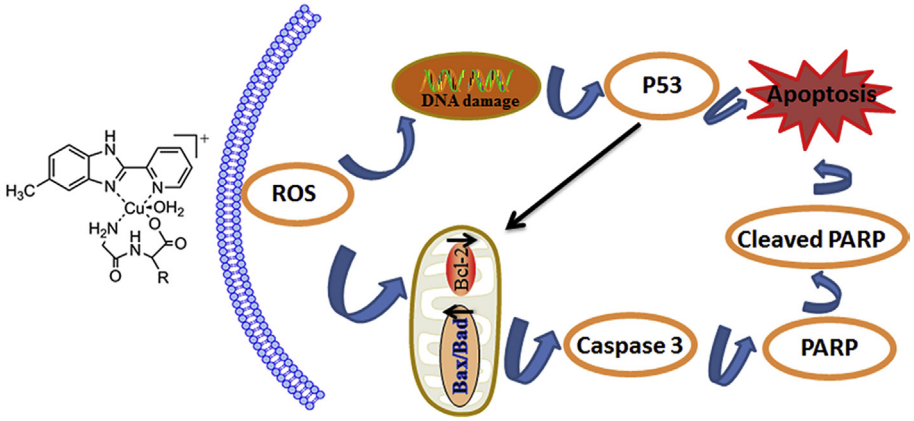

Fig. 11. Proposed anticancer mechanism of the Cu(II) complexes in HeLa cells.

(0.020 g, 0.5 mmol) were mixed in aqueous solution (5 mL) with stirring, followed by addition of $Cu(ClO_4)\cdot 6H_2O$ (0.186 g, 0.5 mmol). Then, methanol solution (20 mL) of HPBM (0.105 g, 0.5 mmol) was added dropwise, and the pH value was adjusted to 4.86 with perchloric acid solution. After being stirred for 1 h at 50 °C, the resulting solutions were filtered and left to evaporate at room temperature to obtain the complexes.

4.3.1. *[Cu(Gly-gly)(HPBM)(H_2O)]ClO_4·0.5H_2O (**1**)*

Yield: 72%. Anal. Calcd for $C_{17}H_{21}N_5O_{8.5}ClCu$: C, 38.49; H, 3.99; N, 13.20%. Found: C, 38.70; H, 3.71; N, 13.00%. FT-IR (KBr, cm^{-1}): ν(−OH) 3412; ν_{as}(−NH_2) 3091; ν_s(−NH_2) 2925; ν_{as}(−COO^-) 1610; ν_s(−COO^-) 1395; ν(C=N) 1456; ν(Cu−O) 626; ν(Cu−N) 420. UV−vis. (MeOH) λ_{nm}/nm, ε/(M^{-1} cm^{-1}): 317, 2.44×10^4; 665, 74.81. Molar conductivity Λ_m (S cm^2 mol^{-1}) in methanol: 89.3. ESI-MS (*m*/*z*, MeOH): 403.9 for $[Cu(Gly\text{-}gly)(HPBM)]^+$. ESR (MeOH): $g_{||} = 2.2784$, $g_{\perp} = 2.0444$.

4.3.2. *[Cu(Gly-L-leu)(HPBM)(H_2O)]ClO_4 (**2**)*

Yield: 75%. Anal. Calcd for $C_{21}H_{28}N_5O_8ClCu$: C, 43.67; H, 4.88; N, 12.13%. Found: C, 43.48; H, 4.59; N, 11.95%. FT-IR (KBr, cm^{-1}): ν(−OH) 3437; ν_{as}(−NH_2) 3082; ν_s(−NH_2) 2960; ν_{as}(−COO^-) 1615; ν_s(−COO^-) 1381; ν(C=N) 1450; ν(Cu−O) 623; ν(Cu−N) 436. UV−vis. (MeOH) λ_{nm}/nm, ε/(M^{-1} cm^{-1}): 323, 2.53×10^4; 677, 64.45. Molar conductivity Λ_m (S cm^2 mol^{-1}) in methanol: 97.8. ESI-MS (*m*/*z*, MeOH): 459.0 for $[Cu(Gly\text{-}L\text{-}leu)(HPBM)]^+$. ESR (MeOH): $g_{||} = 2.2570$, $g_{\perp} = 2.0477$.

4.4. DNA binding and cleavage experiments

Absorption titration experiments were done by maintaining the concentration of the complexes constant and varying CT DNA concentration. The absorption spectra were recorded in the range of 225−500 nm. The base line was corrected by subtracting Tris buffer, and CT DNA was placed to remove the absorbance of the DNA itself. Every experiment was allowed to incubate for 8 min before the spectra were recorded. From the spectroscopic titration data, the binding constants (K_b) were calculated using the following equation (Eq. (1)) [26]:

$$[DNA]/(\varepsilon_a - \varepsilon_f) = [DNA]/(\varepsilon_b - \varepsilon_f) + 1/K_b(\varepsilon_b - \varepsilon_f) \quad (1)$$

where [DNA] is the concentration of DNA in the base pairs. The apparent absorption coefficient ε_a, ε_b and ε_f correspond to A_{obs}/C_{Cu}, the extinction coefficients of the complexes in the bound and free forms, respectively. In plots of $[DNA]/(\varepsilon_a - \varepsilon_f)$ *versus* [DNA], K_b is given by the ratio of the slope $(1/(\varepsilon_b - \varepsilon_f))$ to the intercept $(1/K_b(\varepsilon_b - \varepsilon_f))$.

The competitive experiments were carried out in the buffer (pH 7.2) by maintaining [DNA]/[EB] = 1.25 and varying the concentration of the complexes. Each sample solution was scanned using an excitation wavelength of 525 nm and emission wavelength set at 550−660 nm, and the mixtures were allowed to incubate for 8 min before the spectra were recorded. The Stern−Volmer constants (K_{SV}), a measure of the binding propensity of the complexes to DNA, were calculated using the following equation (Eq. (2)) [30]:

$$I_0/I = 1 + K_{sv}[Q] \quad (2)$$

where I_0 and I stand for the fluorescence intensities at 550−660 nm in the absence and presence of the complexes, respectively. K_{sv} is the linear Sterm−Volmer quenching constant and [Q] is the concentration of the complexes. Additionally, the apparent binding constants (K_{app}) were calculated using the equation (Eq. (3)) [31]:

$$K_{EB}[EB] = K_{app}[complex] \quad (3)$$

where $K_{EB} = 1.0\times10^7\ M^{-1}$, [EB] = 8 μM, and [complex] is the value at 50% decrease of the fluorescence intensity of EB.

CD spectra of CT DNA (100 μM) with the addition of the complexes ([complex]/[DNA] ratios of 0−1.0) were obtained in the range of 220−320 nm at room temperature, using a 10 mm path quartz cuvette. Each spectrum was obtained by averaging three scans and subtracting the background signal of the buffer at 100 nm min^{-1} scanning rate.

All cyclic voltammetric measurements were performed in a single compartment cell with a glass carbon electrode as the working electrode, a Pt wire as the auxiliary electrode and a saturated calomel electrode (SCE) as the reference electrode, at 200 mV s^{-1} scanning rate for the potential range from −0.6 to 0.6 v in buffer solution (pH 7.2) containing 10 mM Tris-HCl/50 mM NaCl as supporting electrolyte. The whole experiments were carried out in a nitrogen atmosphere. The ratios of binding constants of the reduced state Cu(I) and oxidation state Cu(II) were calculated using the following equation (Eq. (3)) [30]:

$$E^{0'}{}_b - E^{0'}{}_f = 0.059\log[K_{Cu(I)}/K_{Cu(II)}] \quad (4)$$

where $E^{0'}{}_b$ and $E^{0'}{}_f$ are the condition potential of Cu(I)/Cu(II) of the complexes alone or in combination with DNA, respectively. And $K_{Cu(I)}$ and $K_{Cu(II)}$ are the corresponding binding constants of the Cu(I) or Cu(II) complexes with DNA, respectively.

The CT DNA viscosity experiments in the absence and presence of EB (standard) or complex **1/2** were conducted on Ostwald Viscometer, immersed in a water bath maintained at 29 ± 0.1 °C. The concentration of CT DNA was 200 μM, and the concentrations of EB and the complexes varied from 0 to 70 μM with 10 μM intervals. The flow times were measured with a digital stopwatch and each sample solution was tested three times to get an average time. Data were presented as $(\eta/\eta_0)^{1/3}$ *versus* r (r = [complex]/[DNA] = 0, 0.05, 0.1, 0.15, 0.20, 0.25, 0.30, 0.35), where η and η_0 are the viscosity of the CT DNA solutions in the absence and presence of the complexes, respectively. The relative viscosity values (η) were calculated based on the observed flow times of the DNA −containing solutions (t) corrected from the flow time of buffer alone (t_0), $\eta = (t\text{-}t_0)/t_0$.

The studies of the complexes docked into DNA were performed using AutoDock Vina1.1.2 set of programs with the Lamarckian Genmetic Algorithm (LGA) [57]. The crystal structure of DNA d(5′-G-Diu-TGCAAC-3′) (PBD ID:454D) was downloaded from the Protein Data Bank, the water molecules were deleted from this structure before performing docking calculations. The molecular structures of the complexes were sketched via Gaussian viewer. A grid box (60, 60, 60) was selected to enclose the whole DNA molecule, with a spacing of grid 0.375 Å, all other parameters were kept at their default setting. The docking results were visualized using PyMol software.

The DNA cleavage was carried out using pBR322 plasmid DNA in Tris buffer (pH 7.2) with the concentrations of the complexes (5−20 μM) and ascorbic acid (50 μM) in a total volume of 10 μL. The samples were incubated for 1 h at 37 °C in the dark. A loading buffer was added, and then electrophoresis was done at 100 V for 40 min in standard Tris-boric acid-EDTA (TBE) buffer (pH 8.3). The obtained gel bands were visualized and photographed using a Gel Imaging System (BIO-RAD Laboratories-Segrate).

In addition, the possible DNA cleavage mechanism of the complexes was investigated in the presence of typical radical scavengers such as hydroxyl radical scavengers (DMSO, ethanol and *tert*-butyl), a superoxide anion radical scavenger (SOD) and a singlet oxygen quencher (NaN_3). Each sample was incubated for 1 h at

37 °C and analyzed according to the procedure as above.

4.5. Antimicrobial test

The antibacterial activity of Gly-gly/Gly-*L*-leu, HPBM, $Cu(ClO_4)_2 \cdot 6H_2O$ and the complexes was tested by oxford cup method as well as broth dilution method respectively. Each experiment was carried out in triplicate, all equipment and culture media were sterilized.

4.5.1. Oxford cup method

The sensitivity of the compounds against different bacterial strains was determined by the oxford cup method with the inhibition zone as the index. Microbial suspensions were diluted in broth medium to obtain 1×10^6 CFU mL^{-1} cell densities. The tested compounds were dissolved in sterile water containing 5% DMSO (2 mg mL^{-1}). Then 100 μL of the compound solution were added to the oxford cups that previously placed on inoculation agar culture. These plates were incubated at 37 °C for 24 h, and the inhibition zone diameter (mm) of each cup was measured.

4.5.2. Broth dilution method

The minimum inhibitory concentration (MIC) and minimum bactericidal concentration (MBC) were measured by the broth dilution method with MTT as the indicator. Microbial cultures were diluted to obtain 1×10^6 CFU mL^{-1}. The tested compounds were dissolved in sterile water containing 5% DMSO (1024, 800 and 640 μg mL^{-1}). Microbial growth was noted by color of the solution in the tubes. Firstly, 1000 μL of broth medium was added to each tube and then tested solution (1000 μL) was mixed with medium in the first tube. Secondly, 1000 μL of mixture from the first tube was transferred to the second tube and so on, to obtain the final concentration ranges of the compounds (512–4, 400–3.125 and 320–2.5 μg mL^{-1}). Then 10 μL of microbial suspension were added to the corresponding tube. The 8th without microbes and the 9th without compounds tube were used as control. After 24 h incubation at 37 °C in shock incubator, 10 μL of MTT solution (5 mg mL^{-1}) was added to each tube and went on cultured for 30 min. The MIC value was defined as the lowest concentration of the compounds that prevent the color from yellow to blue. Then, 20 μL of yellow mixed solution was coated on a nutrient agar medium. Incubated for another 24 h, the lowest concentration without bacterial growth was determined as the MBC value.

4.6. In vitro cytotoxic evaluation

A549, PC-3, HeLa cancer cell lines and LO_2 normal cell lines were seeded into 96-well plates (1×10^4 per well) using RPMI-1640 and DMEM media and cultured in CO_2 incubator (37 °C, 5% CO_2 in air). The cells were treated with the complexes (3.125–200 μM) for 48 h, when they adhered and reached 70–80% confluence. After incubation, the MTT stock solution (20 μL, 5 mg mL^{-1}) was added to each well for an extra 4 h at 37 °C. Later, the medium was discarded, and the formazan crystals were dissolved in DMSO (100 μL). After 10 min of oscillation, the absorbance was measured using a microplate spectrophotometer at 490 nm. Each data was collected three times for calculating the mean and the IC_{50} values (drug concentration which inhibits cell growth by 50%) were calculated to assess the cytotoxic effects of the complexes.

4.7. Anticancer mechanism studies

4.7.1. AO/EB staining technique

HeLa cells (2×10^5 cells/well) were plated and incubated in 12-well plates for 24 h at 37 °C in a 5% CO_2 incubator. After incubation, the cells were treated with the complexes (8.2 μM) for 24 h, and washed two times with cold PBS, and then stained with AO/EB (100 μg mL^{-1}) in the dark for 15 min at 37 °C. After being further washed twice with PBS, the cells samples were detected with an ImageXpress Micro XLS confocal fluorescence microscope.

4.7.2. Annexin V/PI assay

HeLa cells were inoculated overnight in 6-well plates at a density of 4×10^5 cells/well. Then, the complexes (8.2 μM) were added into the well and incubated for another 24 h. After centrifuged (1000 rpm, 6 min) and washed with PBS, the cells were stained with fluorescein isothiocyanate (FITC)-conjugated Annexin V and PI in the dark for 15 min at 37 °C, and then analyzed with a FACS Calibur flow cytometry instrument.

4.7.3. Intracellular reactive oxygen species (ROS) detection

The levels of the ROS in HeLa cells induced by the complexes were measured using the fluorescent dye 2′, 7′-dichlorodihydrofluorescein diacetate (DCFH-DA). The cells were seeded in a 12-well plate with 2×10^5 cells each well, and incubated overnight. After being treated with the complexes (8.2 μM) for 24 h, the cells were washed twice with cold PBS and subsequently pre-stained with DCFH-DA (10 μM) and incubated at 37 °C in the dark for 30 min. Afterward, the treated cells were washed two times with cold PBS, and stained with Hoechest 33 342 for 20 min in the dark at 37 °C. Finally, the cells were washed twice with PBS, and then imaged and quantitatively analyzed using a confocal fluorescence microscope.

4.7.4. Location assay of the complexes and measurement of mitochondrial membrane potential

2×10^5 cells per well were plated on 12-well plates. After 24 h incubation, the complexes (8.2 μM) were added into the wells and incubated for a period of 2, 3, 4 and 5 h, respectively. After being washed two times with cold PBS, the cells were labeled with Mito Tracker® Deep Red FM (80 nM) at 37 °C for 30 min, and then photographed using an ImageXpress Micro XLS system.

HeLa cells were inoculated at a density of 2×10^5 cells/well in 12-well plates and incubated with or without the complexes (8.2 μM) for 24 h at 37 °C, and then washed two times with PBS. Afterward, JC-1 dye (1 μg mL^{-1}) was added and incubated for 20 min in the dark at 37 °C. After being washed with PBS, the cells were suspended in PBS, and observed under an ImageXpress Micro XLS system.

4.7.5. Western blot analysis

HeLa cells were inoculated in 3.5-cm dishes for 24 h and then treated with the complexes (8.2 μM) for another 24-h-incubation. Through being disintegrated and centrifuged (15 min, 13 000 g), the supernatant was collected and the protein concentration was determined by BCA assay. SDS-PAGE (sodium dodecyl sulfate-polyacrylamide gel electrophoresis) was performed by loading equal amount of protein per lane. Gels were then transferred to poly (vinylidene difluoride) membranes (Millipore) and blocked with 5% skim milk powder in TBST containing 0.05% Tween 20 for 5 h. Subsequently, the membranes were incubated with primary antibodies at 1:5000 dilution overnight at 4 °C, and washed four times with TBST for a total of 30 min, then the second antibodies conjugated with horseradish peroxidase at 1:3000 dilution for 65 min at room temperature and washed four times with TBST. The blots were visualized via a chemiluminescence Gel imaging System (FluorChem E, ProteinSimple). The membranes were stripped finally to detect the β-actin in order to evaluate whether the proteins amounts in all the lanes were equal.

4.8. Statistical analysis

All the data were evaluated by using t-tests. The results were expressed as mean ± standard deviations (SD). The differences were considered to be significant when $^{*}P < 0.05$.

Acknowledgements

This work was supported by the Natural Science Foundation of Guangdong Province (No. 2015A030313423).

Appendix A. Supplementary data

Supplementary data related to this article can be found at https://doi.org/10.1016/j.ejmech.2018.05.023.

References

[1] A.K. Renfrew, Metallomics 6 (2014) 1324–1335.
[2] R.P. Paitandi, S. Mukhopadhyay, R.S. Singh, V. Sharma, S.M. Mobin, D.S. Pandey, Inorg. Chem. 56 (2017) 12232–12247.
[3] A. Bergamo, P.J. Dyson, G. Sava, Coord. Chem. Rev. 360 (2018) 17–33.
[4] D. Wan, B. Tang, Y.J. Wang, B.H. Guo, H. Yin, Q.Y. Yi, Y.J. Liu, Eur. J. Med. Chem. 139 (2017) 180–190.
[5] C. Marzano, M. Pellei, F. Tisato, C. Santini, Anti Canc. Agents Med. Chem. 9 (2009) 185–211.
[6] F. Tisato, C. Marzano, M. Porchia, M. Pellei, C. Santini, Med. Res. Rev. 30 (2010) 708–749.
[7] C. Santini, M. Pellei, V. Gandin, M. Porchia, F. Tisato, C. Marzano, Chem. Rev. 114 (2014) 815–862.
[8] P.R. Reddy, N. Raju, Polyhedron 44 (2012) 1–10.
[9] D. Inci, R. Aydin, O. Vatan, T. Sevgi, D. Yilmaz, Y. Zorlu, Y. Yerli, B. Cosut, E. Demirkan, N. Cinkilic, J. Biol. Inorg. Chem. 22 (2017) 61–85.
[10] S.T. Chew, K.M. Lo, S.K. Lee, M.P. Heng, W.Y. Teoh, K.S. Sim, K.W. Tan, Eur. J. Med. Chem. 76 (2014) 397–407.
[11] Z. Boulsourani, S. Katsamakas, G.D. Geromichalos, V. Psycharis, C.P. Raptopoulou, D. Hadjipavlou-Litina, E. Yiannaki, C. Dendrinou-Samara, Mater. Sci. Eng. C 76 (2017) 1026–1040.
[12] Z.Y. Ma, Z. Qiao, D.B. Wang, X. Hou, X. Qiao, C.Z. Xie, Z.Y. Qiang, J.Y. Xu, Appl. Organomet. Chem. 31 (2017) e3651.
[13] M. Badea, I.D. Vlaicu, R. Olar, M. Constand, C. Bleotu, M.C. Chifiriuc, L. Marutescu, V. Lazar, M.N. Grecu, D. Marinescu, J. Therm. Anal. Calorim. 118 (2014) 1119–1133.
[14] J.A. Zhao, H.B. Yu, S.C. Zhi, R.N. Mao, J.Y. Hu, X.X. Wang, Chin. Chem. Lett. 28 (2017) 1539–1546.
[15] J.Y. Hu, Y. Guo, J.A. Zhao, J.S. Zhang, Bioorg. Med. Chem. 25 (2017) 5733–5742.
[16] A.A. Ei-Sherif, B.J.A. Jeragh, Spectrochim. Acta, Part A 68 (2007) 877–882.
[17] G. Kumaravel, P.P. Utthra, N. Raman, Bioorg. Chem. 77 (2018) 269–279.
[18] I. Castillo, M. Suwalsky, M.J. Gallardo, V. Troncoso, B.N. Sanchez-Eguia, E. Santiago-Osorio, I. Aguiniga, A.K. Gonzalez-Ugarte, J. Inorg. Biochem. 156 (2016) 98–104.
[19] S. Tabassum, W.M. Al-Asbahy, M. Afzal, M. Shamsi, F. Arjmand, J. Lumin. 132 (2012) 3058–3065.
[20] A. Gutierrez, I. Marzo, C. Cativiela, A. Laguna, M.C. Gimeno, Chem. Eur J. 21 (2015) 11088–11095.
[21] B. Warzajtis, B.D. Glisic, N.D. Savic, A. Pavic, S. Vojnovic, A. Veselinovic, J. Nikodinovic-Runic, U. Rychlewska, M.I. Djuran, Dalton Trans. 46 (2017) 2594–2608.
[22] Y. Gou, J.L. Li, B.Y. Fan, B.H. Xu, M. Zhou, F. Yang, Eur. J. Med. Chem. 134 (2017) 207–217.
[23] G. Facchin, N. Veiga, M.G. Kramer, A.A. Batista, K. Varnagy, E. Farkas, V. Moreno, M.H. Torre, J. Inorg. Biochem. 162 (2016) 52–61.
[24] F. Arjmand, A. Jamsheera, D.K. Mohapatra, J. Photochem. Photobiol., B 121 (2013) 75–85.
[25] S. Iglesias, N. Alvarez, M.H. Torre, E. Kremer, J. Ellena, R.R. Ribeiro, R.P. Barroso, A.J. Costa, M.G. Kramer, G. Facchin, J. Inorg. Biochem. 139 (2014) 117–123.
[26] X.B. Fu, Z.H. Lin, H.F. Liu, X.Y. Le, Spectrochim. Acta, Part A 122 (2014) 22–33.
[27] K.E. Prosser, S.W. Chang, F. Saraci, P.H. Le, C.J. Walsby, J. Inorg. Biochem. 167 (2017) 89–99.
[28] X.B. Fu, G.T. Weng, D.D. Liu, X.Y. Le, J. Photochem. Photobiol., A 276 (2014) 83–95.
[29] Q. Gan, X.B. Fu, W.J. Chen, Y.H. Xiong, Y.L. Fu, S. Chen, X.Y. Le, J. Fluoresc. 26 (2016) 905–918.
[30] Q. Gan, Y.Y. Qi, Y.H. Xiong, Y.L. Fu, X.Y. Le, J. Fluoresc. 27 (2017) 701–714.
[31] X.B. Fu, J.J. Zhang, D.D. Liu, Q. Gan, H.W. Gao, Z.W. Mao, X.Y. Le, J. Inorg. Biochem. 143 (2015) 77–87.
[32] W.J. Geary, Coord. Chem. Rev. 7 (1971) 81–122.
[33] B.S. Garg, D.N. Kumar, M. Sarbhai, Spectrochim. Acta, Part A 61 (2005) 141–147.
[34] E. Manoj, M.R.P. Kurup, A. Punnoose, Spectrochim. Acta, Part A 72 (2009) 474–483.
[35] S.K. Tadavi, J.D. Rajput, S.D. Bagul1, A.A. Hosamani, J.N. Sangshetti, R.S. Bendre, Res. Chem. Intermed. 43 (2017) 4863–4879.
[36] X.B. Fu, D.D. Liu, Y. Lin, W. Hu, Z.W. Mao, X.Y. Le, Dalton Trans. 43 (2014) 8721–8737.
[37] P.R. Reddy, N. Raju, B. Satyanarayana, Chem. Biodivers. 8 (2011) 131–144.
[38] H. Sigel, Inorg. Chem. 14 (1975) 1535–1540.
[39] M. Zampakou, S. Balala, F. Perdih, S. Kalogiannis, I. Turel, G. Psomas, RSC Adv. 5 (2015) 11861–11872.
[40] C. Protogeraki, E.G. Andreadou, F. Perdih, I. Turel, A.A. Pantazaki, G. Psomas, Eur. J. Med. Chem. 86 (2014) 189–201.
[41] F. Arjmand, M. Muddassir, I. Yousuf, J. Photochem. Photobiol., B 136 (2014) 62–71.
[42] Saswati, A. Chakraborty, S.P. Dash, a. K. Panda, R. Acharyya, A. Biswas, S. Mukhopadhyay, S.K. Bhutia, A. Crochet, Y.P. Patil, M. Nethajie, R. Dinda, Dalton Trans. 44 (2015) 6140–6157.
[43] K.C. Skyrianou, F. Perdih, A.N. Papadopoulos, I. Turel, D.P. Kessissoglou, G. Psomas, J. Inorg. Biochem. 105 (2011) 1273–1285.
[44] C.J. Dhanaraj, J. Johnson, Mater. Sci. Eng. C Mater. Biol. Appl. 78 (2017) 1006–1015.
[45] M. Jiang, Y.T. Li, Z.Y. Wu, Z.Q. Liu, C.W. Yan, J. Inorg. Biochem. 103 (2009) 833–844.
[46] L.H. Abdel-Rahman, A.M. Abu-Dief, H. Moustafa, S.K. Hamdan, Appl. Organomet. Chem. 31 (2017) e3555.
[47] M.N. Patel, H.N. Joshi, C.R. Patel, Spectrochim. Acta, Part A 104 (2013) 48–55.
[48] T.S. Lobana, S. Indoria, A.K. Jassal, H. Kaur, D.S. Arora, J.P. Jasinski, Eur. J. Med. Chem. 76 (2014) 145–154.
[49] N.S. El-Gohary, M.I. Shaaban, Eur. J. Med. Chem. 137 (2017) 439–449.
[50] V.T. Yilmaz, C. Icsel, F. Suyunova, M. Aygun, B. Cevatemre, E. Ulukaya, New J. Chem. 41 (2017) 8092–8106.
[51] A. Gaal, V.G. Mihucz, S. Bosze, I. Szabo, M. Baranyi, P. Horvath, C. Streli, N. Szoboszlai, Microchem. J. 136 (2018) 227–235.
[52] X.L. Hong, Y.H. Zhou, C.C. Zeng, X.C. Wu, Y.J. Liu, J. Organomet. Chem. 846 (2017) 312–320.
[53] B. Tang, D. Wan, S.H. Lai, H.H. Yang, C. Zhang, X.Z. Wang, C.C. Zeng, Y.J. Liu, J. Inorg. Biochem. 173 (2017) 93–104.
[54] X. Sun, M. Liu, L.Y. Gao, Y. Mao, D.M. Zhao, J.F. Zhuang, L. Liu, Eur. J. Med. Chem. 150 (2018) 719–728.
[55] R. Schiffmann, A. Neugebauer, C.D. Klein, J. Med. Chem. 49 (2006) 511–522.
[56] M.E. Reichmann, S.A. Rice, C.A. Thomas, P. Doty, J. Am. Chem. Soc. 76 (1954) 3047–3053.
[57] O. Trott, A.J. Olson, J. Comput. Chem. 31 (2010) 455–461.